Electronic Supplementary Material (ESI) for Nanoscale.

Supporting Information

Do Quantum Interference Effects Manifest in Acyclic Aliphatic Molecules with Anchoring Groups?

Ravinder Kumar,[a] Charu Seth,*[b] Ravindra Venkatramani*[a] and Veerabhadrarao Kaliginedi*[b]

[a] Department of Chemical Sciences, Tata Institute of Fundamental Research (TIFR), Mumbai 400005, India

[b] Department of Inorganic and Physical Chemistry, Indian Institute of Science (IISc), Bangalore 560012, India

Email: charu15.seth@gmail.com, ravi.venkatramani@tifr.res.in, vkaliginedi@iisc.ac.in

S1. Methods

The molecules were built in GaussView6 and energy minimized using density functional theory (DFT) with a B3LYP exchange correlation functional and a 6-311+G(d,p) basis set in Gaussian 16 package. For each energy minimized molecular geometry, the electronic structure for obtaining the Hamiltonian in molecular orbital basis was computed using PM7[1,2] semi-empirical method implemented in Gaussian 16 package. We used non-equilibrium Green's function (NEGF) formalism[3–6] for computing the thermopower (charge transport properties) of the molecules considered in this work using a custom-built MATLAB code. The conductance of all the molecules is calculated using Landauer's formula:

$$G = \frac{2q}{hV}\int_{-\infty}^{\infty} dE\, T(E)\left[f_L(E) - f_R(E)\right] \#(S1)$$

and the expression of thermopower $S(T)$, which can be derived from the Landauer's formula, is given by Eqn. (S2).[6]

$$S(T) = -\frac{1}{eT}\frac{\int_{-\infty}^{\infty} dE\, T(E)(E-\mu)\left(-\frac{\partial f}{\partial E}\right)}{\int_{-\infty}^{\infty} dE\, T(E)\left(-\frac{\partial f}{\partial E}\right)} \#(S2)$$

where T is the temperature; μ is the chemical potential; f is the fermi function; $T(E)$ is the transmission function of energy E; e is the electronic charge; and E_F is the Fermi energy.

Herein, we briefly describe the NEGF formalism[3,4] applied in this work. The molecular junction is considered to be divided into three subsystems—left electrode, molecule, and right electrode. The Green's function for the molecular junction—which is the solution of the inhomogeneous Schrodinger's equation in the presence of charge-injecting electrodes—describes the molecule as well as its interactions with the electrodes; this function is written as follows (Eqn. (S3)).

$$G(E) = \frac{1}{EI - H - \left(\Sigma_L + \Sigma_R\right)} \#(S3)$$

Where H is the Hamiltonian matrix of the isolated molecule obtained using semi-empirical electronic structure method. $\Sigma_{L/R}$ is the self-energy term corresponding to the left (L) / right (R) electrode; this term describes the influence of electrodes on the molecule, which could be of two types: shifting or broadening the molecular energy levels. The real part of the self-energy corresponds to a shift and the imaginary part corresponds to a broadening of the molecular energy levels. The broadening matrix is given as (Eqn. (S4)).

$$\Gamma_{L/R} = i\left(\Sigma_{L/R} - \Sigma_{L/R}^{\dagger}\right) \#(S4)$$

The focus of the current work is on the characteristics of the isolated molecule, so the electrodes are considered structureless.[3,4] Therefore, these *virtual* electrodes are only considered to broaden the molecular energy levels, and the shift due to them is considered

zero. The pathways for charge transport are summed up and constitute the quantity called transmission coefficient, which is computed as per Eqn. (S5).

$$T(E) = Tr\left(\Gamma_L G \Gamma_R G^{\dagger}\right) \#(S5)$$

The broadening is applied only to anchoring group atoms in the basis of atomic orbitals. For example, if the anchoring group is amine, the broadening is applied to the valence s- and p-orbitals of N atoms; if the anchoring group is thiol (or selenol), the broadening is applied to the valence s- and p-orbitals of S (or Se) atoms. For this purpose, the basis of the Hamiltonian was converted from molecular orbital to atomic orbital. Here we assume the weak-coupling limit,[3] within which the molecular levels are only broadened by the electrode (and hence weakly affected) and the coupling among the molecular levels is not affected by the electrodes. This allows one to study the molecular junction in terms of the isolated molecular properties. Mathematically, the elements of the broadening matrix (in the atomic orbital basis) are represented by Eqn. (S6a–S6c).

$\Gamma_{ii} = \gamma$ for the valence orbitals of anchoring group atoms $(S6a)$

$\Gamma_{ii} = 0$ otherwise $(S6b)$

$\Gamma_{ij} = 0$ when $i \neq j$ $(S6c)$

Where i and j are the atomic orbital indices of the anchoring group atoms; γ is the anchor-group–electrode coupling parameter used in our calculation, whose value has been fixed to a small constant, $0.1\ eV$.

We do not explicitly model the electrodes[3,4,7] because the exact atomic arrangement of atoms in the electrodes around the molecule is not precisely known; in fact, in MCBJ or STM-BJ experiments, the electrodes are made to undergo multiple cycles of collision and retraction, thereby leading to a different electrode geometry (at the sites that bind to the molecules) each time. The variation in the coordination geometry of the electrodes is one of the factors responsible for the spread in experimental conductance and thermopower values. The calculations reported in the literature often assume a pyramidal structure of the electrode. Rather than explicit modeling the electrodes, which is computationally expensive, we have simplified our calculations by assuming a small average effect of the electrodes by

adopting broadening matrices. This assumption worked well in explaining experimental conductance data for a variety of molecules previously.[3,4]

S2. Justification of electronic structure methods

We have used semi-empirical method PM7[1,2] for computing the electronic structure of the molecules under investigation. Compared to the ab initio methods, semi-empirical methods are relatively computationally inexpensive and moderately accurate, so they provide a reasonable bargain between accuracy and computational cost.[2,8–10] Several other studies have demonstrated the use of semi-empirical method INDO/S for computing the electronic structure.[11–14] However, the Hamiltonians computed using PM6 and PM7 methods have shown dramatic improvement in accuracy over those computed using older semi-empirical methods: MNDO, AM1, PM3, and INDO/S.[15] Nevertheless, for the sake of comparison with density functional theory (using B3LYP exchange correlation functional and 6-311+G(d,p) basis set), we also show DFT-computed NDMOs I and II in Fig. S5: they are very similar to the PM7-calculated MOs (shown in Fig. S4) but have slightly larger lobes, which is understandable as DFT tends to overestimate the electron density. It is to be noted, however, that we have not used DFT-calculated MOs to compute the transmission probability spectra. This is because within the computational framework that we have adopted, we first convert the molecular orbitals to atomic orbitals and then apply the coupling to the anchor group atoms in the atomic basis. Since DFT involves calculation of electron density and not real molecular orbitals, their conversion to 'fictitious' atomic orbitals is injudicious. Nonetheless, the analysis carried out in the manuscript will not be impacted by the differences in PM7 and DFT generated electronic structure.

Please note that while semi-empirical methods are known to overestimate the HOMO–LUMO gap,[10] DFT is known to underestimate the HOMO–LUMO gap. For alkanedithiols, PM7 gives a gap value of ~9 eV, whereas DFT gives a gap value of ~6 eV. Therefore, it is safe to assume that the gap lies between 6 eV and 9 eV.

S3. Details of the molecular orbital energies

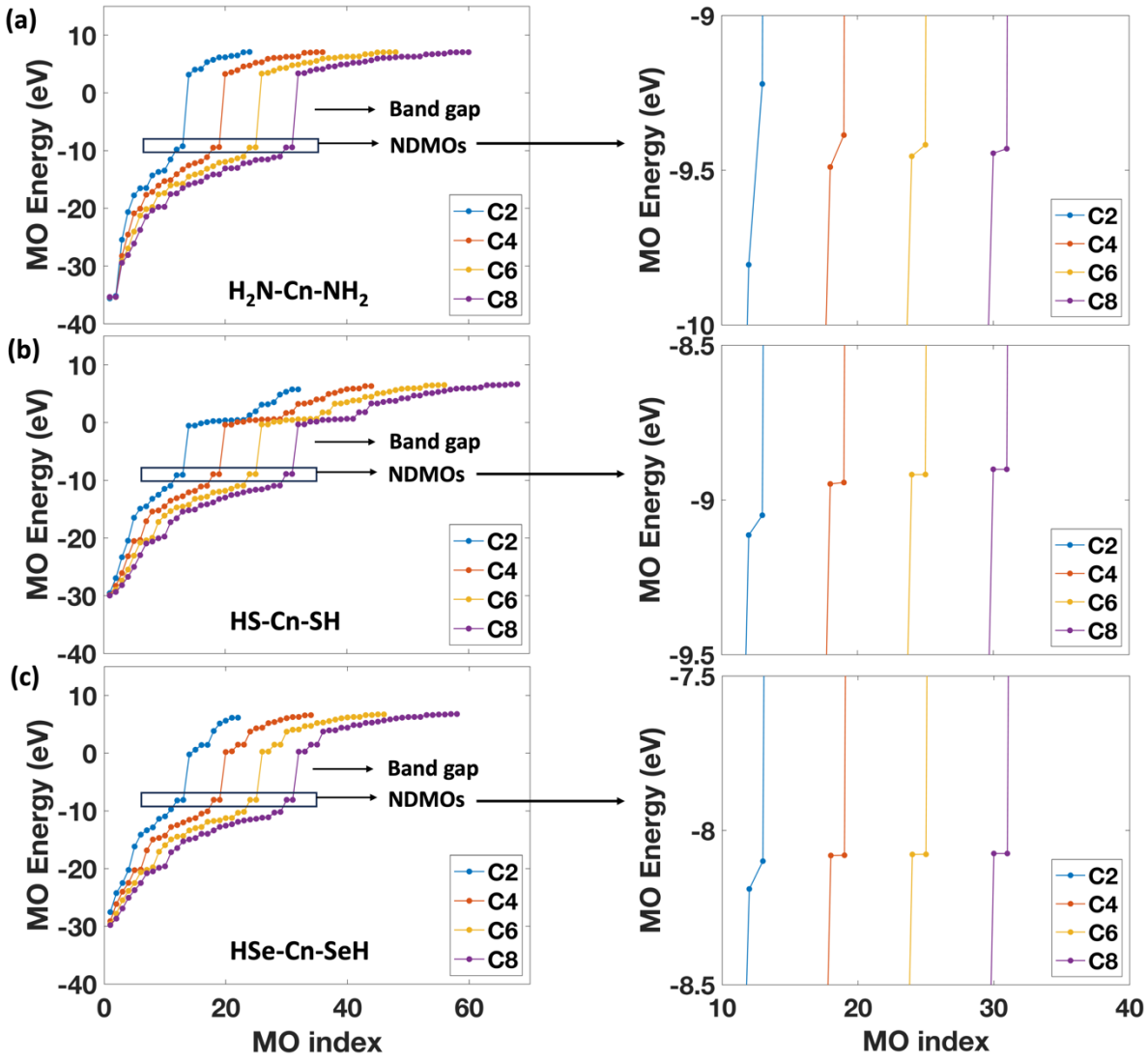

Figure S1. MO energies (computed using the semi-empirical PM7 method) of C2, C4, C6, and C8 (**a**) alkanediamines, (**b**) alkanedithiols, and (**c**) alkanediselenols. Right panels in **a**–**c** show the zoomed plot to clearly visualize and compare NDMOs energies.

Table S1. Energies (computed using the semi-empirical PM7 method) of the near-degenerate molecular orbitals (NDMOs) in C2–C8 ADTs, ADAs, and ADSs. E_I and E_{II} are the energies for NDMO I and NDMO II respectively.

Chain Length	**Dithiols**		**Diamines**		**Diselenols**	
	E_I **(**eV**)**	E_{II} **(**eV**)**	E_I **(**eV**)**	E_{II} **(**eV**)**	E_I **(**eV**)**	E_{II} **(**eV**)**
C2	−9.0497	−9.1136	–9.2211	–9.8053	–8.0995	–8.1898
C4	−8.9436	−8.9482	–9.3863	–9.4897	–8.0804	–8.0812
C6	−8.9177	−8.9183	–9.4175	–9.4549	–8.0772	–8.0777
C8	−8.9011	−8.9011	–9.4304	–9.4451	–8.0747	–8.0747

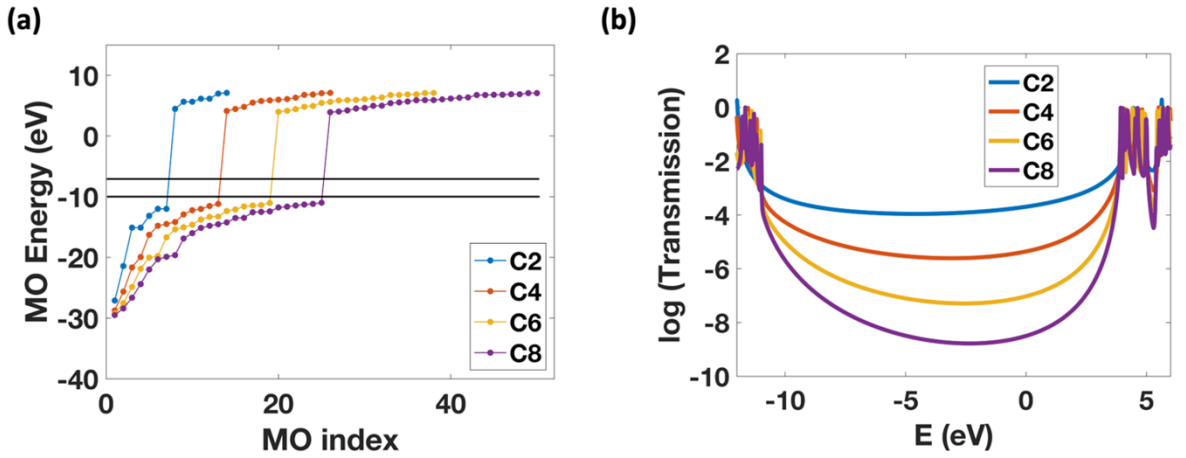

Figure S2. MO energies (computed using the semi-empirical PM7 method) of C2, C4, C6, and C8 alkanes as a function of MO index. Note the absence of MOs between two horizontal black lines indicating absence of NDMOs in alkane systems. **(b)** Logarithmic transmission for C2, C4, C6, and C8 alkanes. The HOMO–LUMO gaps for C8, C6, and C4 are similar (14.8 eV, 14.9 eV, and 15.2 eV, respectively) as reflected in the MO energies and transmission peaks. The HOMO–LUMO gap for C2 (ca. 16.5 eV) is higher than the rest.

S4. Details of the NDMOs

Herein, visual depiction of NDMOs is shown for the specified molecules to demonstrate on which atoms the electron density is present and to what extent.

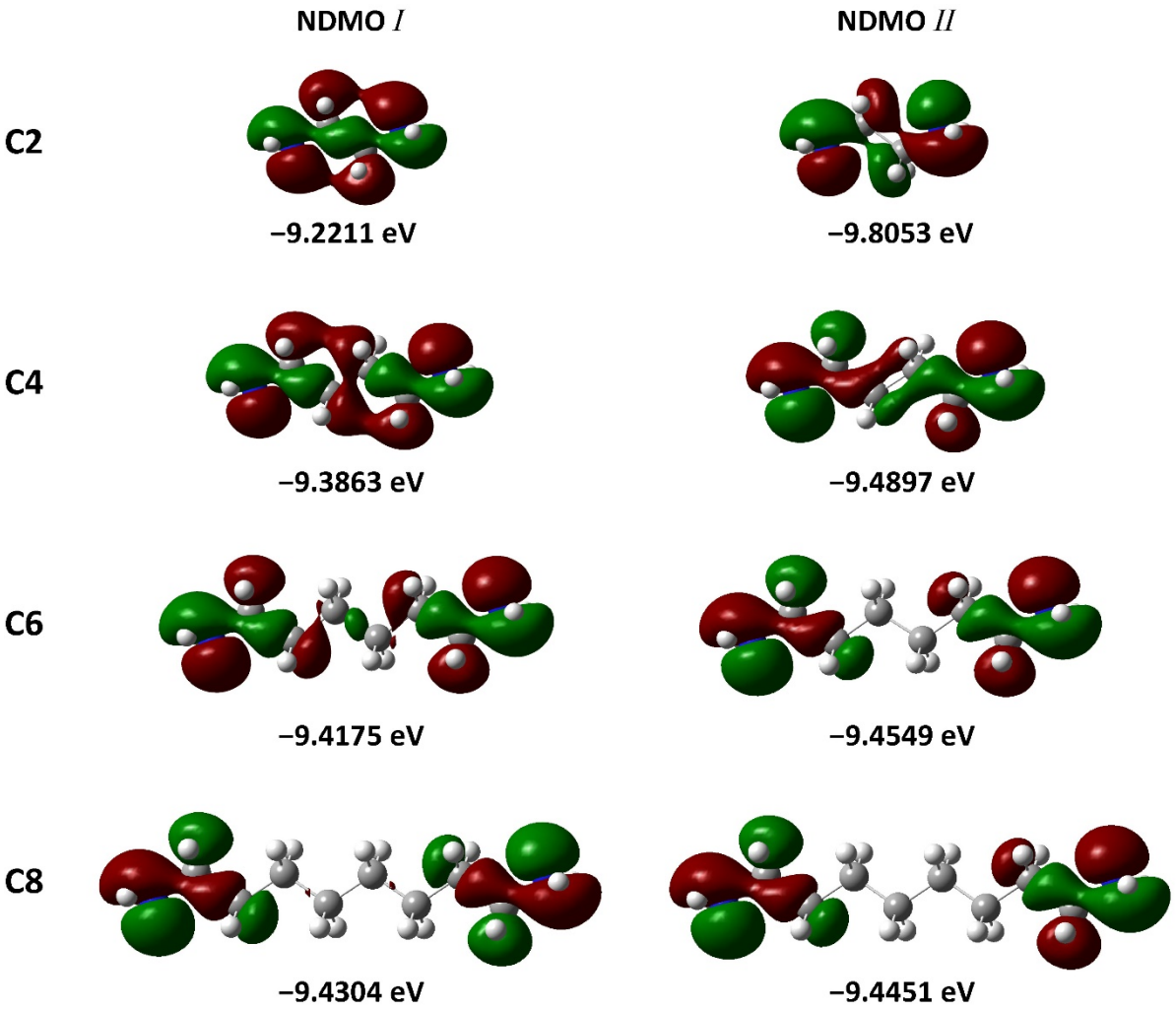

Figure S3. NDMOs of alkanediamines C2, C4, C6, and C8 computed using PM7. NDMOs I are slightly higher in energy than corresponding NDMOs II. Majority of electron density lies on the terminal amine groups, with small but significant electron density on adjacent carbons as well.

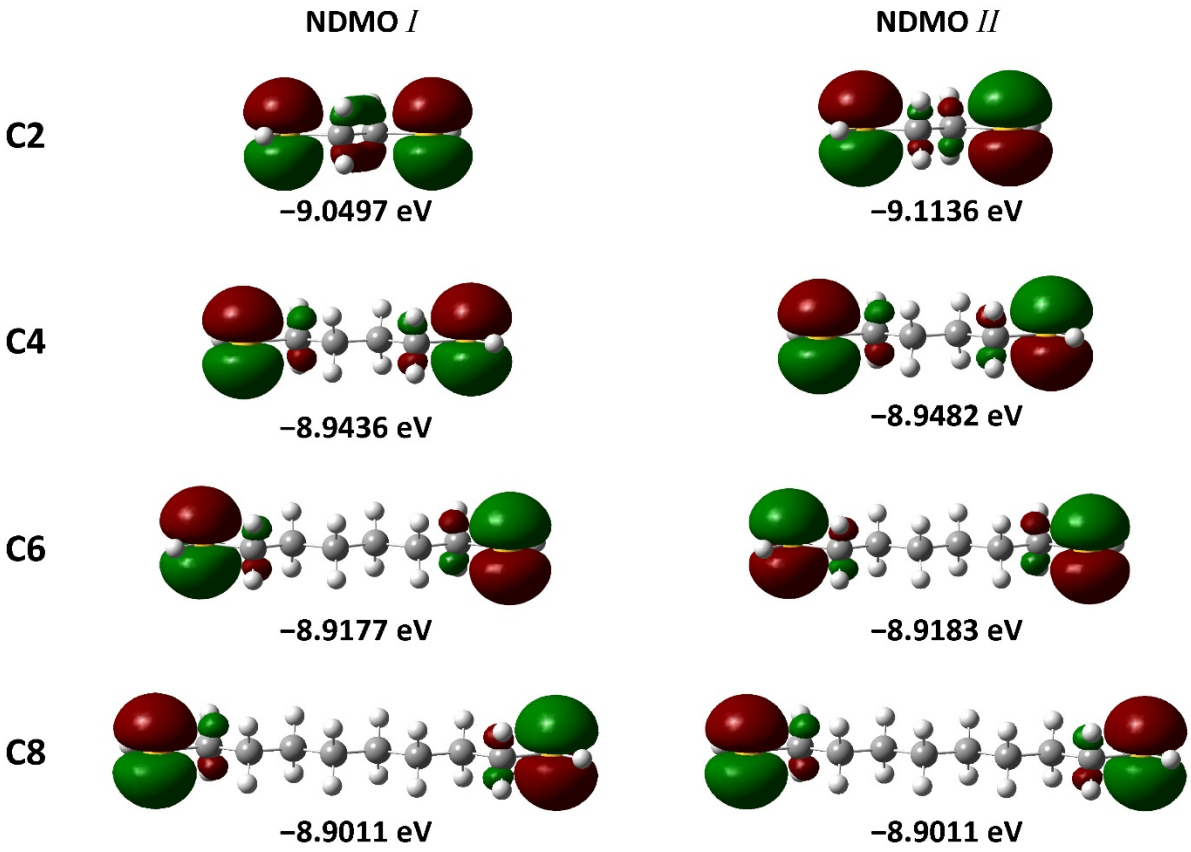

Figure S4. NDMOs of alkanedithiols C2, C4, C6, and C8 computed using PM7. NDMOs I are slightly higher in energy than corresponding NDMOs II. Majority of electron density lies on the terminal thiol groups, with small electron density on adjacent carbons, which is much lower in magnitude than that observed in the case of alkanediamines (Fig. S3).

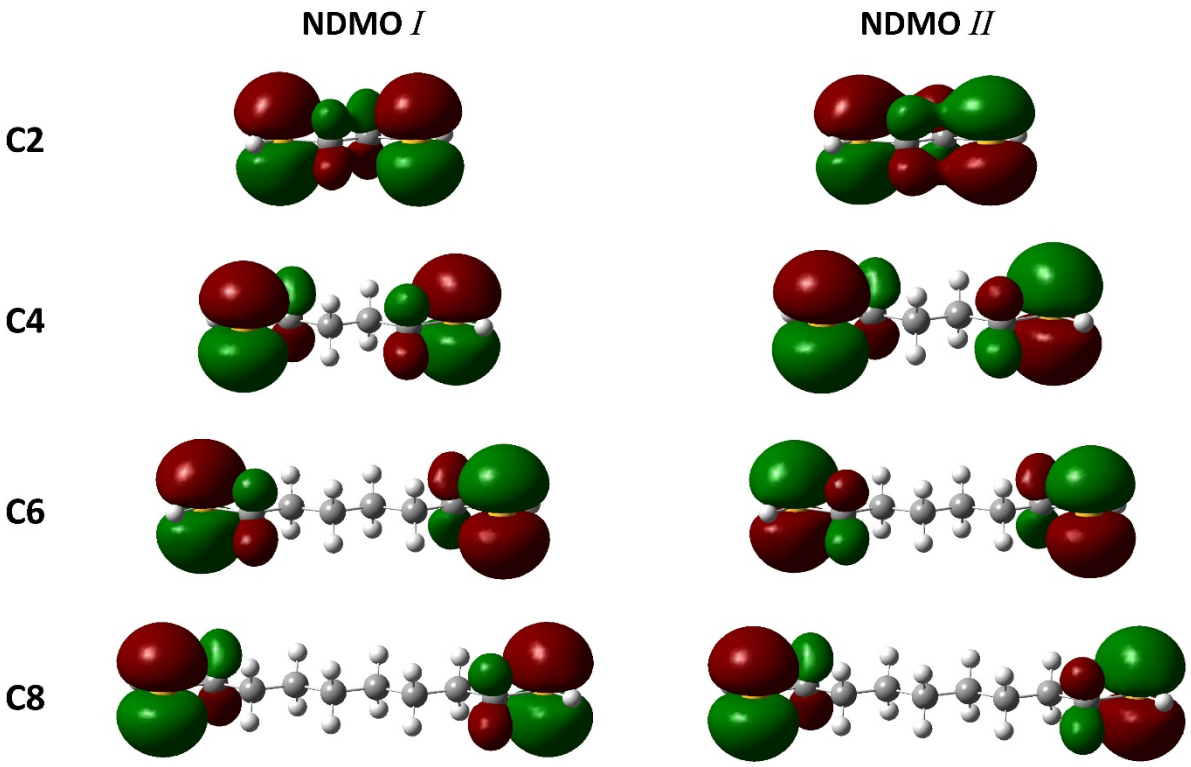

Figure S5. NDMOs of alkanedithiols C2, C4, C6, and C8, computed using DFT (B3LYP functional, 6-311+G(d,p) basis set). NDMOs I are slightly higher in energy than corresponding NDMOs II. Majority of electron density lies on the terminal thiol groups, with small electron density on adjacent carbons. Comparing these with PM7-computed NDMOs, the relative electron density on carbon w.r.t. to thiol is higher in the DFT-NDMOs, which reflects the over-conjugating nature of DFT.

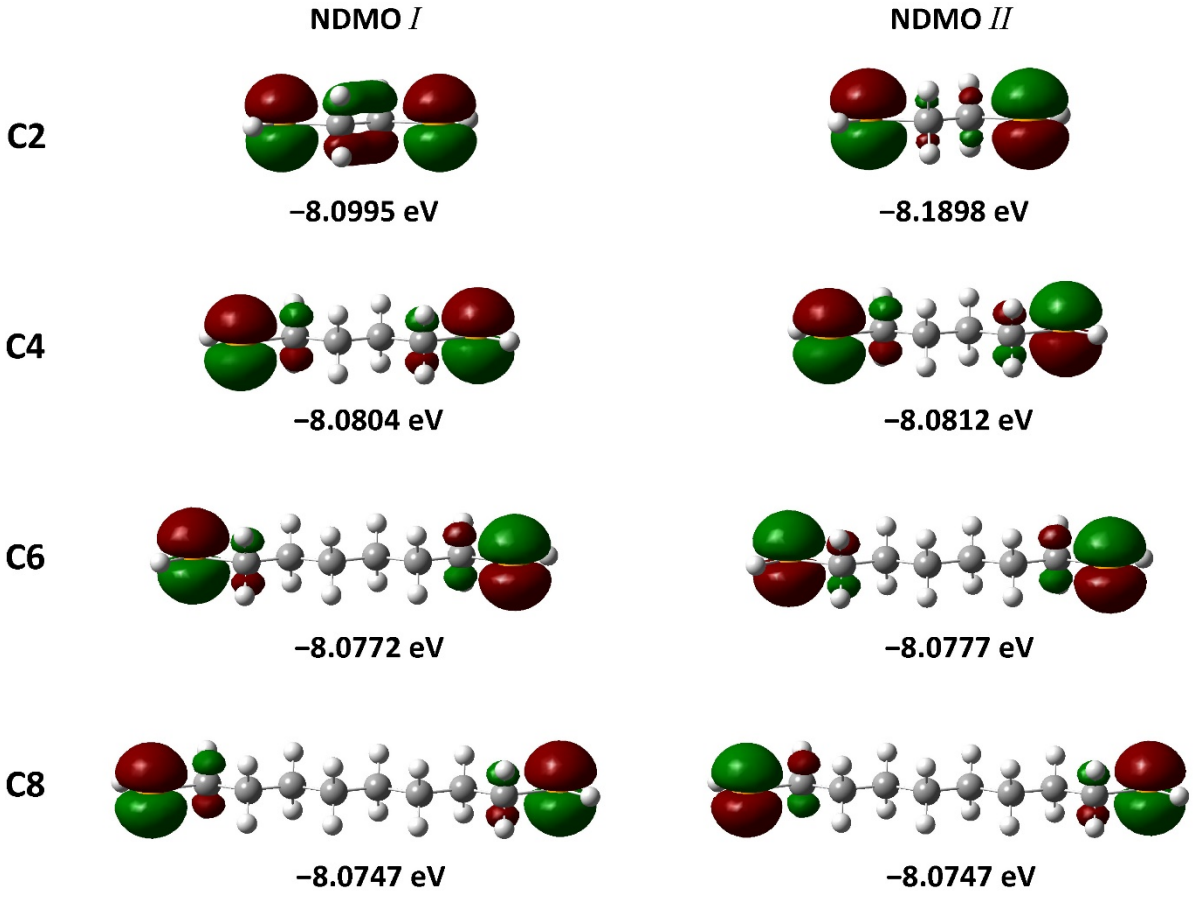

Figure S6. NDMOs of alkanediselenols C2, C4, C6, and C8 computed using PM7. NDMOs I are slightly higher in energy than corresponding NDMOs II. Majority of electron density lies on the terminal selenol groups, with small electron density on adjacent carbons, which appears very similar in magnitude to that observed in the case of alkanedithiols (Fig. S4).

S5. Q-factor Analysis

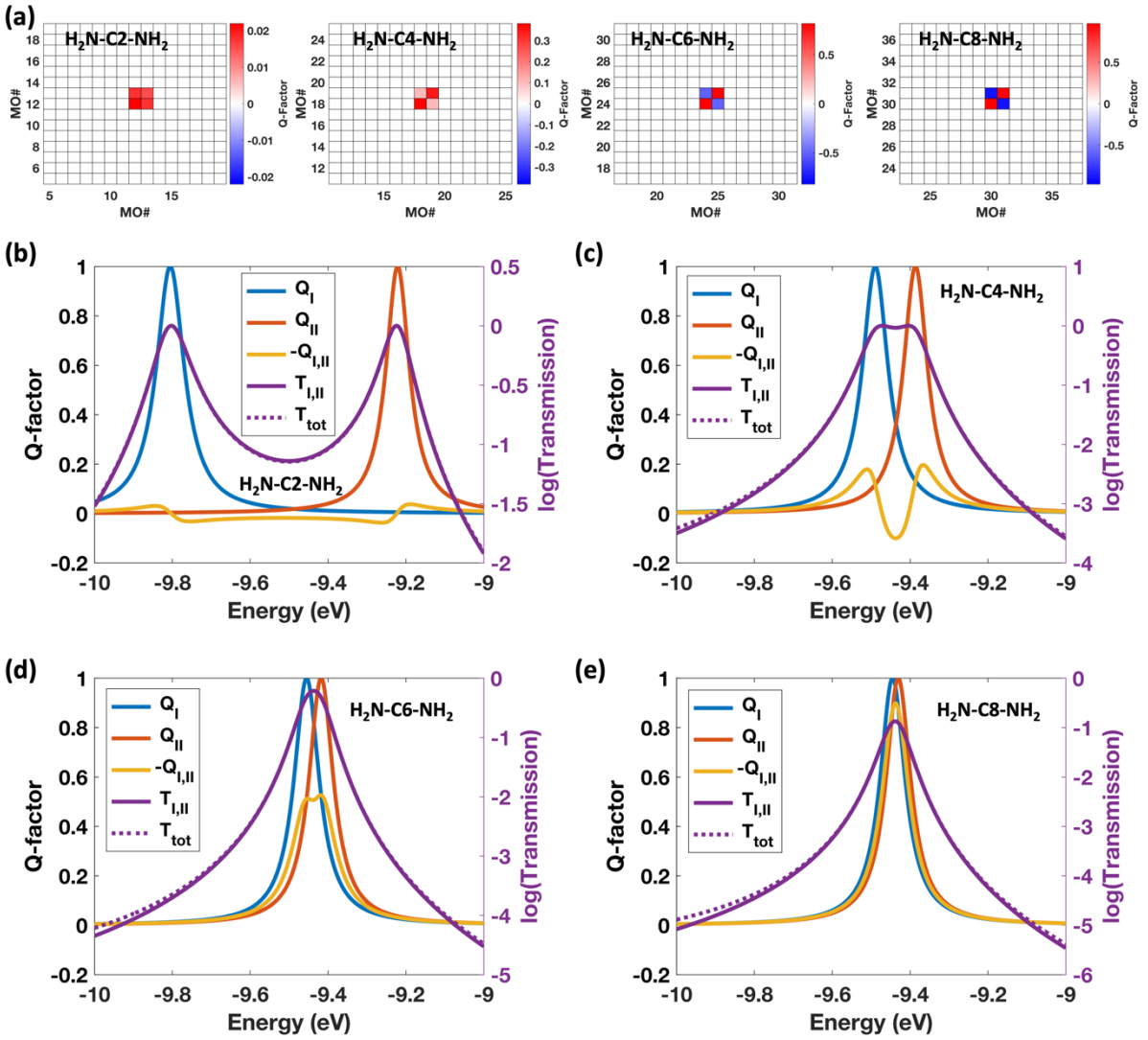

Figure S7. (a) Q-matrix heatmaps for C2–C8 alkanediamines showing NDMO *I* and *II* have major pure and QI contributions to the transmission at mid-point energy between the NDMOs energies. For C2 and C4 diamines, there is manifestation of CQI between NDMOs; whereas for C6 and C8, there is manifestation of DQI between NDMOs. **(b)–(e)** Q-factors for NDMO *I* and *II* (red, blue, and yellow lines), transmission from NDMO *I* and *II* (solid magenta line)**,** and total transmission (dashed magenta line) for C2–C8 alkanediamines plotted in the vicinity of NDMOs energies. Blue, red, and yellow lines are plotted on left y-axis; while magenta lines are plotted on right y-axis.

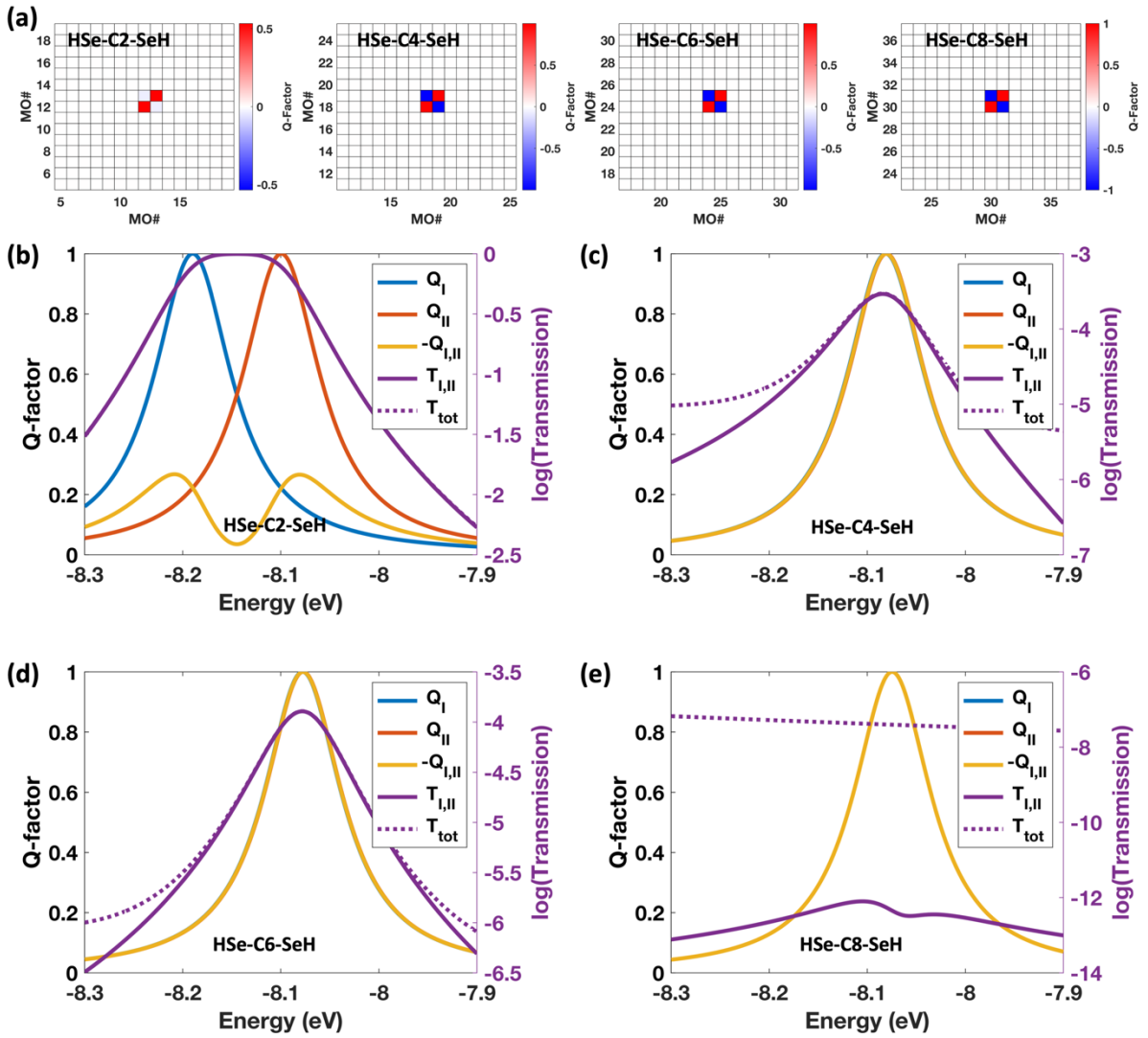

Figure S8. (a) Q-matrix heatmaps for C2–C8 alkanediselenols showing NDMO *I* and *II* have major pure and QI contributions to the transmission at mid-point energy between the NDMOs energies. **(b)–(e)** Q-factors for NDMO *I* and *II* (red, blue, and yellow lines), transmission from NDMO *I* and *II* (solid magenta line), and total transmission (dashed magenta line) for C2–C8 alkanediamines plotted in the vicinity of NDMOs energies. Blue, red, and yellow lines are plotted on left y-axis; while magenta lines are plotted on right y-axis.

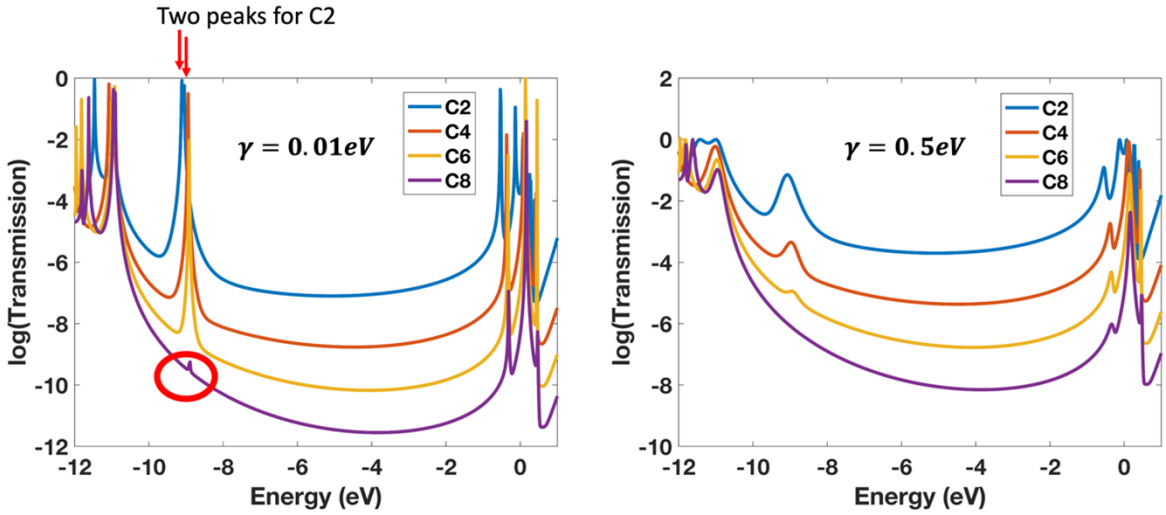

Figure S9. Transmission of alkanedithiols C2, C4, C6, and C8 computed using a low value of coupling parameter $\gamma = 0.01\ eV$ and a high value of coupling parameter $\gamma = 0.5\ eV$. For $\gamma = 0.01\ eV$, C2 shows two peaks in the gap feature and there is appearance of small peaks in the gap feature for C8 molecule. For $\gamma = 0.5\ eV$, all the peaks are broadened and intensity of the peaks decreases.

S6. Accessing Gap Feature in Experimental Setup

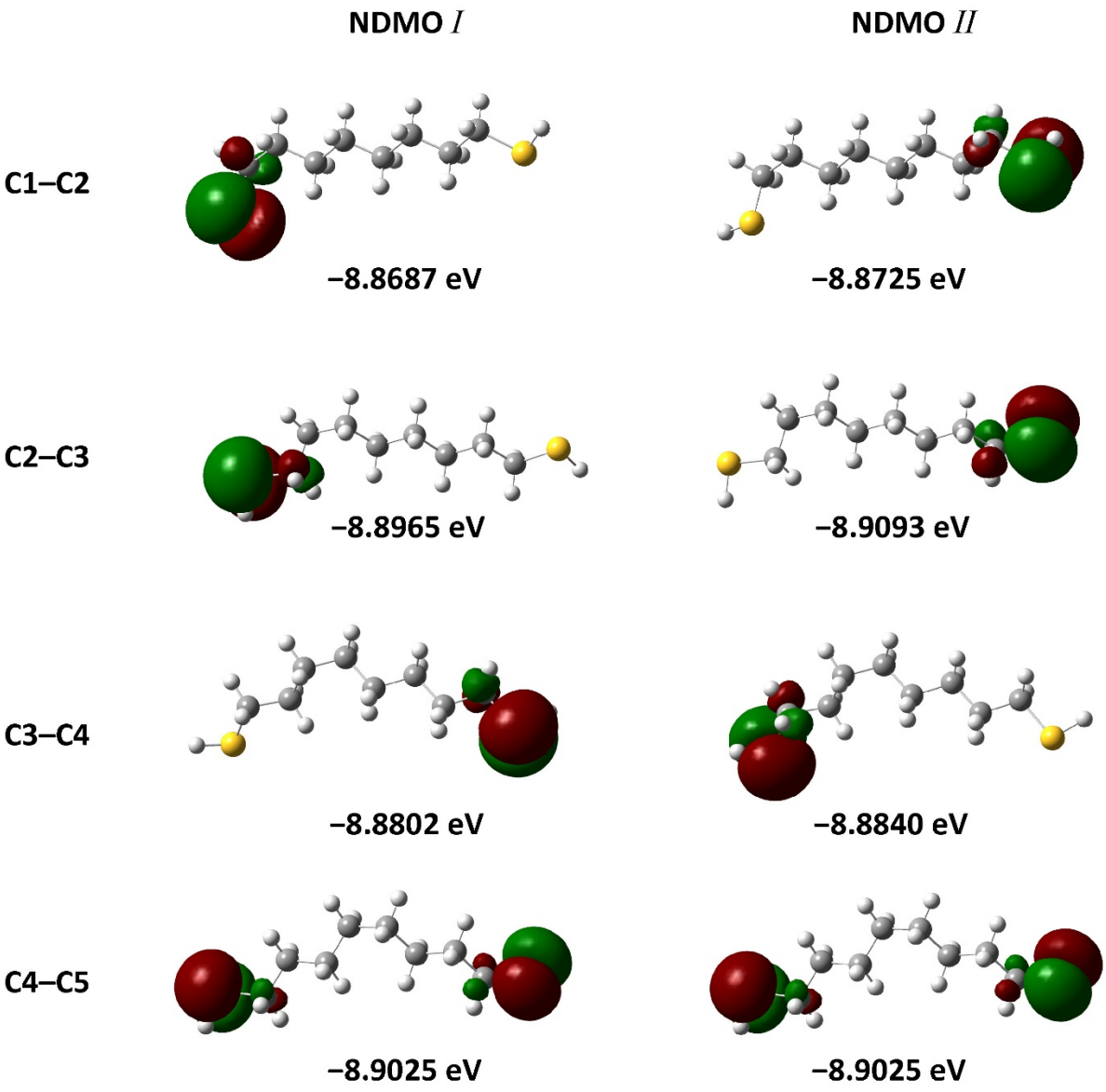

Figure S10. NDMOs corresponding to C1–C2, C2–C3, C3–C4, and C4–C5 gauche-defected C8 dithiol structures.

Table S2. NDMO energies (computed using the semi-empirical PM7 method) of gauche-defected C8 dithiol molecules as well as the energy offset $\Delta E_{I,II}$ between the NDMOs.

C8 dithiol molecule with gauche-defect at:	**Energy of NDMO I (eV)**	**Energy of NDMO II (eV)**	**Energy offset ($\Delta E_{I,II}$) between NDMOs I and II (eV)**
C1–C2	−8.8687	−8.8725	0.0038
C2–C3	−8.8965	−8.9093	0.0128
C3–C4	−8.8802	−8.8840	0.0038
C4–C5	−8.9025	−8.9025	0.0000

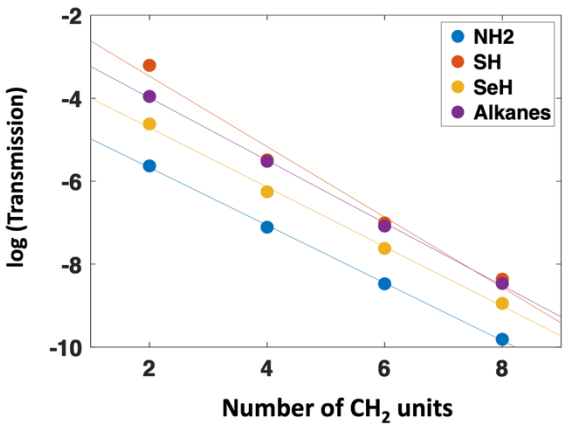

Figure S11. Logarithmic transmission as a function of chain-length for ADAs, ADTs, ADSs, and alkanes. Note that this data was obtained for $E_f = -5.1eV$.

Table S3. Thermopower values for ADAs, ADTs, and ADSs systems studied here at $E_f = -5.1eV$. Note that the data is not in accordance with experiments.[16] This is likely because the thermopower distance dependence is very sensitive to the nature of MIGS[16,17] which are only partially captured in our calculations which do not model the electrodes explicitly.

Chain Length	**Amines** S **(μV/K)**	**Thiols** S **(μV/K)**	**Selenols** S **(μV/K)**
C2	1.46	0.09	0.68
C4	3.00	1.10	1.63
C6	4.28	2.06	2.61
C8	5.18	3.00	3.61

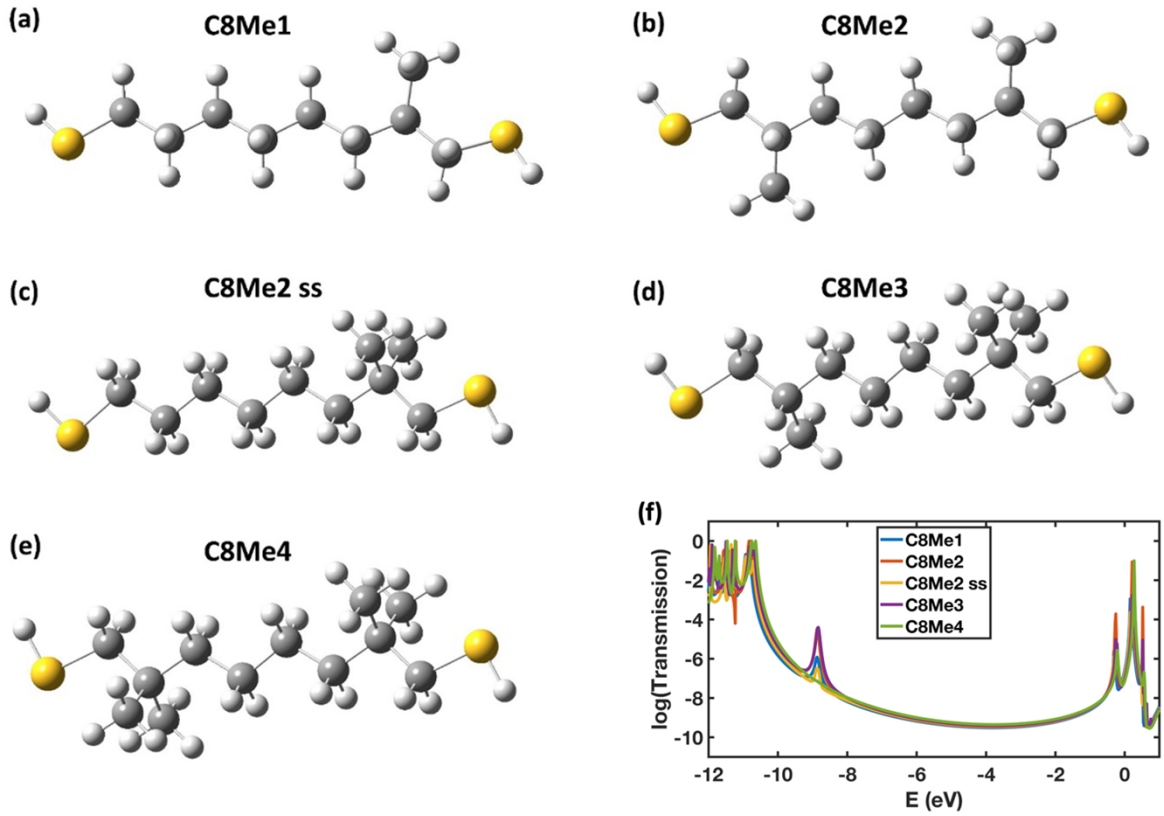

Figure S12. (a)–(e) Molecular structures of C8 dithiol with beta-methyl-substitution(s); the numeral after Me in the label denotes the number of methyl group substitutions made on the beta carbon of C8 dithiol; 'ss' denotes 'same side' to distinguish C8Me2 from C8Me2 ss. **(f)** Transmission probability spectra of the molecules shown in (a)–(e).

References

1 M. I. Bernal-Uruchurtu and M. F. Ruiz-López, *Chem Phys Lett*, 2000, **330**, 118–124.

2 C. Brückner, 2017.

3 Y. Xing, T. H. Park, R. Venkatramani, S. Keinan, D. N. Beratan, M. J. Therien and E. Borguet, *J Am Chem Soc*, 2010, **132**, 7946–7956.

4 C. Seth, V. Kaliginedi, S. Suravarapu, D. Reber, W. Hong, T. Wandlowski, F. Lafolet, P. Broekmann, G. Royal and R. Venkatramani, *Chem Sci*, 2017, **8**, 1576–1591.

5 S. Datta, *Quantum Transport : Atom to Transistor, Cambridge University Press*, 2005.

6 L. Rincó n-Garcí, ab Charalambos Evangeli, G. Rubio-Bollinger ac and N. Agraı, *Chem. Soc. Rev*, 2016, **45**, 4285.

7 K. Yoshizawa, T. Tada and A. Staykov, *Journal of American Chemical Society*, 2008, **130**, 9406–9413.

8 F. Jensen, *Introduction to Computational Chemistry*, John Wiley & Sons Ltd., Chichester, 2nd edn., 2007.

9 A. S. Christensen, T. Kubař, Q. Cui and M. Elstner, *Chem Rev*, 2016, **116**, 5301–5337.

10 J. Mato and E. B. Guidez, *J Phys Chem A*, 2020, **124**, 2601–2615.

11 E. Wierzbinski, A. de Leon, X. Yin, A. Balaeff, K. L. Davis, S. Reppireddy, R. Venkatramani, S. Keinan, D. H. Ly, M. Madrid, D. N. Beratan, C. Achim and D. H. Waldeck, *J Am Chem Soc*, 2012, **134**, 9335–9342.

12 E. Hatcher, A. Balaeff, S. Keinan, R. Venkatramani and D. N. Beratan, *J Am Chem Soc*, 2008, **130**, 11752–11761.

13 Y. Xing, T.-H. Park, R. Venkatramani, S. Keinan, D. N. Beratan, M. J. Therien and E. Borguet, *J Am Chem Soc*, 2010, **132**, 7946–7956.

14 A. Paul, S. Bezer, R. Venkatramani, L. Kocsis, E. Wierzbinski, A. Balaeff, S. Keinan, D. N. Beratan, C. Achim and D. H. Waldeck, *J Am Chem Soc*, 2009, **131**, 6498–6507.

15 R. L. M. Gieseking, M. A. Ratner and G. C. Schatz, *J Phys Chem A*, 2018, **122**, 6809–6818.

16 S. Park, N. Cho and H. J. Yoon, *Chemistry of Materials*, 2019, **31**, 5973–5980.

17 S. Park, J. Jang and H. J. Yoon, *Journal of Physical Chemistry C*, 2021, **125**, 20035–20047.